ACS Catalysis

pubs.acs.org/acscatalysis

Research Article

In Situ Strong Metal–Support Interaction (SMSI) Affects Catalytic Alcohol Conversion

Felipe Polo-Garzon,* Thomas F. Blum, Zhenghong Bao, Kristen Wang, Victor Fung, Zhennan Huang, Elizabeth E. Bickel, De-en Jiang, Miaofang Chi, and Zili Wu*

Cite This: *ACS Catal.* 2021, 11, 1938–1945

Read Online

ACCESS | Metrics & More | Article Recommendations | Supporting Information

ABSTRACT: Strong metal–support interactions (SMSIs) and catalyst deactivation have been heavily researched for decades by the catalysis community. The promotion of SMSIs in supported metal oxides is commonly associated with H_2 treatment at high temperature (>500 °C), and catalyst deactivation is commonly attributed to sintering, leaching of the active metal, and overoxidation of the metal, as well as strong adsorption of reaction intermediates. Alcohols can reduce metal oxides, and thus we hypothesized that catalytic conversion of alcohols can promote SMSIs *in situ*. In this work we show, via IR spectroscopy of CO adsorption and electron energy loss spectroscopy (EELS), that during 2-propanol conversion over Pd/TiO_2 coverage of Pd sites occurs due to SMSIs at low reaction temperatures (as low as ∼190 °C). The emergence of SMSIs during the reaction (*in situ*) explains the apparent catalyst deactivation when the reaction temperature is varied. A steady-state isotopic transient kinetic analysis (SSITKA) shows that the intrinsic reactivity of the catalytic sites does not change with temperature when SMSI is promoted *in situ*; rather, the number of available active sites changes (when a TiO_x layer migrates over Pd NPs). SMSI generated during the reaction fully reverses upon exposure to O_2 at room temperature for ∼15 h, which may have made their identification elusive up to now.

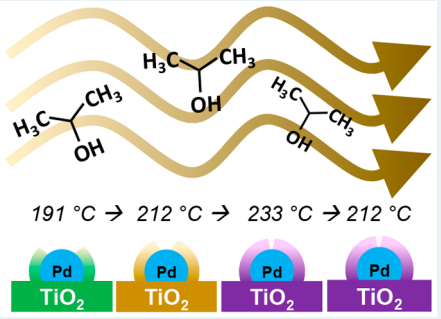

KEYWORDS: *strong metal–support interaction, alcohol conversion, supported-metal catalysts, acid–base catalysis, FTIR, EELS, SSITKA*

INTRODUCTION

The catalytic conversion of alcohols is an important chemical process that enables the transformation of bioderived intermediates into chemical products currently supplied in great extent by the oil industry. One of the great challenges for diversifying the sources for chemicals of mass consumption, i.e. unlocking the commercial viability of bioderived products, is fundamentally understanding the transformation of active sites under *operando* conditions that lead to decreased reaction rates. Typical *operando* reconstructions of the active sites that lead to catalyst deactivation are sintering, leaching of the active metal (especially in slurry-phase reactions), and overoxidation of the metal, as well as strong adsorption of reaction intermediates or carbonaceous species.[1−3]

For metal nanoparticles (NPs) supported on metal oxides, strong metal–support interactions (SMSIs) can cause decreased rates. SMSI refers to the migration of the support over the metal NPs, which reduces the number of exposed metal catalytic sites. This phenomenon is commonly induced in metal oxide supports by treatment in H_2 (≥500 °C).[4−8] Recent reports have deepened the understanding of this phenomenon. For instance, it has been shown that alloying of the supported NP with metal atoms in the support is a mechanism competing with the migration of the overlayer.[9] In addition, the size of the supported metal particle/cluster affects the SMSI, with larger NPs promoting SMSI more easily than smaller NPs, supported clusters, and single atoms.[10−12] Oxygen treatment[13] and a wet-chemistry methodology[14] have also been reported to induce SMSI.

When it is properly harnessed, SMSI can lead to improved catalytic performance compared with the base metal–support system (without SMSI). The existence of SMSI can improve catalyst stability with time on stream,[5,15−18] increase turnover frequency,[19] and steer reaction selectivity.[18,20] In our previous work,[21] it was shown that, upon exposure of Au/TiO_2 to 2-propanol at 150 °C, nearly 95% of the Au sites were covered due to carbonaceous deposits and/or SMSI. Intrigued by this phenomenon, we hypothesized that alcohol conversion over noble metals supported on reducible supports might strongly affect the nature of the active sites due to *in situ* SMSIs. Pd supported on reducible supports is a commonly used catalyst for the conversion of a variety of alcohols.[22−24] Thus, we have decided to use the dehydrogenation/dehydration of 2-

Received: December 4, 2020
Revised: January 11, 2021
Published: January 28, 2021

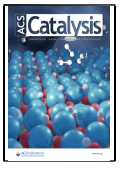

https://dx.doi.org/10.1021/acscatal.0c05324
ACS Catal. 2021, 11, 1938–1945

propanol to acetone/propene over Pd/TiO_2 as a model system to study the effect of potential *in situ* SMSI on catalysis. We believe our findings will help reimagine the nature of active sites on other Pd catalysts where a reducing reactive mixture is present.[25−28]

In the present work, steady-state isotopic transient kinetic analysis (SSITKA), IR spectroscopy of CO adsorption, electron energy loss spectroscopy (EELS), transmission electron microscopy (TEM), and temperature-programmed oxidation are combined to show that the *in situ* occurrence of SMSI during 2-propanol conversion at low temperature (as low as 190 °C) leads to partial coverage of Pd sites by a TiO_x layer, thus altering the nature of the active sites and hampering reaction rates. The overlayer coating on Pd NPs easily reverses at room temperature, which has probably made its identification elusive to date.

EXPERIMENTAL DETAILS

Synthesis of Pd/TiO_2. Deposition−precipitation with urea (DPU) was used to deposit Pd NPs on TiO_2. This procedure has been reported before,[29−31] and our implementation is described as follows. Titanium dioxide anatase (Sigma-Aldrich, 99.9+%) was calcined in air at 400 °C for 5 h prior to use. Palladium chloride ($PdCl_2$, Aldrich, 99.999%) was used as the precursor for Pd NPs. $PdCl_2$ (in the amount required to achieve the desired theoretical loading, 2.2 wt %) was mixed with 1 g of TiO_2 and 100 mL of water. Urea (Sigma-Aldrich, 99.5%) was added at a 2.5/1 urea/TiO_2 wt/wt ratio. In addition, NH_4Cl was added at a wt/wt ratio NH_4Cl to $PdCl_2$ of 6/1 to increase the solubility of $PdCl_2$ in water. The mixture was heated to 85 °C and maintained at that temperature using a heating mantle while it was stirred continuously at 1200 rpm for 16 h. After 16 h, the solution was centrifuged at 12000 rpm for 10 min to separate the catalyst. The catalyst was washed with deionized water and the centrifuge−wash cycle was repeated five times. The catalyst was dried overnight in a vacuum oven at 60 °C and subsequently calcined in air at 300 °C for 5 h.

Inductively Coupled Plasma (ICP), Surface Area, and X-ray Diffraction (XRD). Inductively coupled plasma atomic emission spectroscopy (ICP-AES) was performed by Galbraith Laboratories Inc. The loading of Pd in the sample was 0.35 wt %. Brunauer−Emmett−Teller (BET) surface areas were measured using a Micromeritics Gemini VII Surface Area and Porosity Analyzer at −196 °C. The surface area of TiO_2 anatase was 9.1 m^2/g. The BET surface area of 0.35 wt % Pd/TiO_2 anatase was measured to be 10.2 m^2/g. X-ray diffraction (XRD) data were collected with a PANalytical Empyrean system using Cu Kα radiation. Diffraction patterns were collected at incident angles for 2θ = 5−90°. Both TiO_2 and Pd/TiO_2 showed the titania anatase phase (Figure S1).

IR Spectroscopy. Spectra were collected using a Thermo Nicolet Nexus 670 FTIR spectrometer with an MCT detector. Each spectrum was recorded with 32 scans at a resolution of 4 cm^{-1}. The sample was loaded in a ceramic cup, which was placed in a diffuse reflectance infrared Fourier transform spectroscopy (DRIFTS) cell (Pike Technologies). The sample was treated under different gas atmospheres: O_2 (30 mL/min of 3% O_2/Ar), 2-propanol (30 mL/min of 6% 2-propanol/Ar), and Ar (30 mL/min). CO adsorption/desorption was performed at 30 °C. Background spectra were collected at 30 °C after treatment of the catalyst sample and before CO was adsorbed. After treatment in O_2 or 2-propanol, the catalyst was flushed in Ar for 10 and 30 min at 300 °C, respectively. When consecutive treatment−CO adsorption cycles were performed, CO was fully desorbed from Pd sites at 300 °C (Figure S2).

Microscopy. The sample was treated *ex situ* in 2-propanol at 300 °C and cooled to room temperature. The sample was then either briefly exposed to air or kept in air for 1 month before transferring into the chamber of the NION UltraSTEM 100 kV microscope. The electron energy loss spectroscopy (EELS) data were collected using a Gatan Enfina spectrometer with a dispersion of 0.2 eV, convergence and collection semiangles of 30 and 48 mrad, respectively, and a dwell time of 500 ms. The zero-loss peak had a full-width at half maximum of 1 eV.

Transmission electron microscopy (TEM) images to characterize the particle-size distribution were acquired using a JEOL NEOARM instrument operated at 80 kV.

DFT Calculations. The Vienna ab initio simulation package (VASP)[32,33] was employed to perform periodic density functional theory (DFT) calculations. The Perdew−Burke−Ernzerhof (PBE)[34] functional with the generalized-gradient approximation (GGA) was used for electron exchange and correlation. The projector-augmented wave method (PAW)[35,36] was used to describe the electron−core interaction. The tolerance for force convergence was 0.05 eV/Å. All calculations were spin-polarized. A vacuum layer of 15 Å was used between slabs. The bottom two layers were fixed during optimization. To model the covered Pd surface due to SMSI, a monolayer of Ti_2O_3 (001) in a 2 × 2 cell was placed on the Pd (111) surface to simulate a reduced titanium oxide layer.

Kinetic Measurements. Catalysts were pretreated at 295 °C in 50 mL/min 5% O_2/Ar for 5 h before catalytic tests were performed in a homemade plug-flow reactor system. Catalyst particles (30 mg) were diluted in quartz beads at a quartz/catalyst ratio of 12 (w/w). Both the catalyst and the quartz were sieved to 177−250 μm. The mixture was loaded into a microreactor and held in place by quartz wool. A Nexus 3000 syringe pump (Chemyx) was used to inject 0.6−4 μL/min of 2-propanol into the system. Ar was used as the carrier for 2-propanol. The reaction products were identified and quantified using a Buck Scientific Model 910 gas chromatograph (GC) with a MXT-Q-BOND column. All kinetic experiments were performed under differential conditions (conversion <13%). Steady-state isotopic transient kinetic analysis (SSITKA) was performed to measure the turnover frequencies (TOF, rate per active site) of the catalyst at different temperatures and quantify the density of surface intermediates.[37−39] The reaction was allowed to reach a steady state under "regular conditions": 2-propanol (CH_3CH_3CHOH) in 2% Ne/He (Ne was the tracer accounting for the gas-phase hold-up in the system). Once a steady state was reached, the inlet of the reactor was changed to labeled 2-propanol ($^{13}CH_3{}^{13}CH_3CHOH$) in 2% Ar/He while the reaction conditions were held constant (flow, concentration, temperature, pressure). The observed kinetic isotopic effect was not significant. The transient concentrations of reactants and products were monitored using a mass spectrometer (MS) (Pfeiffer Vacuum OmniStar). MS signals followed were m/z 20 (Ne), 40 (Ar), 39 (propene), 45 (2-propanol), and 58 and 60 (acetone). The contributions from different components to a single mass were decoupled and subtracted. To obtain the real surface residence times (τ_0), the surface residence time (τ) was

https://dx.doi.org/10.1021/acscatal.0c05324
ACS Catal. 2021, 11, 1938−1945

measured at different gas space velocities (30, 50, 100, 200 L g^{-1} h^{-1}) for each temperature evaluated. τ_0 is the surface residence time as the total flow approaches infinity.

Temperature-Programmed Desorption (TPD). TPD experiments were performed with a commercial Altamira Instruments system (AMI-300). A 5 mg portion of the catalyst sample was loaded into a U-tube quartz reactor. Before TPD experiments, the sample was treated in 50 mL/min of 5% O_2/He and (sometimes) in 50 mL/min of 6% 2-propanol/He (He bubbled through saturator), and CO_2 or NH_3 was adsorbed on the catalyst surface at 30 °C (45 mL/min of 10% CO_2/Ar for 2 h or 45 mL/min of 2% NH_3/He for 2 h). TPD experiments were performed in the temperature range 40−895 °C at a ramping rate of 10 °C/min. The outlet from the reactor was analyzed using an MS instrument (Pfeiffer Vacuum OmniStar). The masses followed were m/z 18 (H_2O), 28 (CO), 41 (propene), 44 (CO_2), 17 (NH_3), 45 (2-propanol), and 58 (acetone). The contributions from different components to a single mass were decoupled and subtracted.

Temperature-Programmed Oxidation (TPO). TPO experiments were performed in a commercial Altamira Instruments system (AMI-300). A 15 mg portion of the catalyst sample (particle size <177 μm) was loaded into a U-tube quartz reactor. Before TPO experiments, the sample was treated in 50 mL/min of 5% O_2/He and in 50 mL/min of 6% 2-propanol/He (He bubbled through a saturator). TPO experiments were performed in the temperature range 40−895 °C at a ramping rate of 10 °C/min. The outlet from the reactor was analyzed using a MS instrument (Pfeiffer Vacuum OmniStar).

RESULTS AND DISCUSSION

Blockage of Pd Sites after Treatment in 2-Propanol. Exposed Pd sites were probed via DRIFTS after CO adsorption at 30 °C (Figure 1). Initially, the sample was treated in O_2 at 300 °C to identify the Pd sites available for CO adsorption before any SMSI (migration of the TiO_2 support over the Pd NPs) was induced. Linear CO adsorption on oxidized $Pd^{\delta+}$ (2148 cm^{-1}), atop CO adsorption on Pd(111) defects (2089 cm^{-1}), and on bridge (1973 cm^{-1}) and 3-fold (1894 cm^{-1}) adsorption sites were identified (Figure 1).[40] When the sample was treated in 2-propanol at 100 °C, the adsorption of CO was reduced by ∼80%. 2-Propanol treatment at 300 °C reduced the available Pd sites by ∼90%. Adsorption on positively charged Pd sites ($Pd^{\delta+}$) disappeared completely after treatment in 2-propanol, due to reduction of Pd sites. These results suggest the blockage of surface sites of Pd NPs, which would be consistent with SMSI and/or carbonaceous deposits. Next, we explored the stability of the coating overlayer upon exposure to O_2 at 30 °C.

Reversibility of the Blockage. *DRIFTS.* As treatment in 2-propanol at 300 °C leaves carbonaceous species (adsorbed isopropoxy, adsorbed acetone, adsorbed propene, acetates, and carbonates) on the surface (Figure S3), it is reasonable to think that these adsorbates may be related to the blockage of surface Pd sites and thus diminished the signal during DRITFS of CO adsorption. Figure 2a-1st shows the adsorption of CO at 30 °C after blockage of Pd sites was induced via 2-propanol treatment at 300 °C. Next, CO was desorbed in Ar at 300 °C, followed by readsorption at 30 °C (Figure 2a-1nd). The number of exposed sites increased 2.6 times due to the removal of carbonaceous species upon desorption of CO (see Figure S4). However, when the same procedure was repeated but exposure

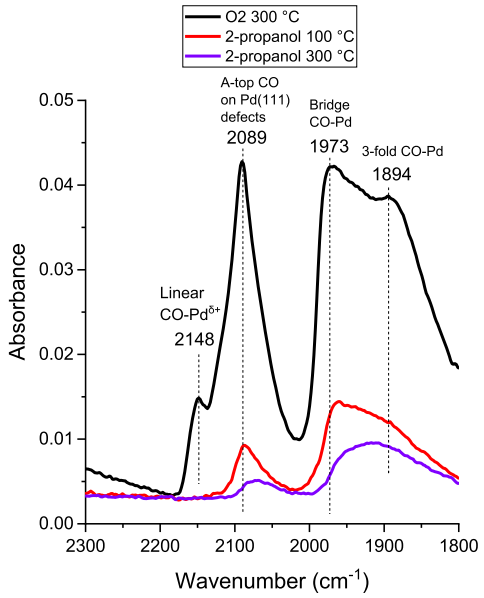

Figure 1. DRIFTS of adsorbed CO (after 10 min desorption) at 30 °C on Pd/TiO_2 after treatment in O_2 at 300 °C and in 2-propanol at 100 and 300 °C (in that order). CO was desorbed in O_2 at 300 °C before the next treatment. The sample was flushed in Ar at 300 °C after each treatment. All spectra were collected for the same sample load.

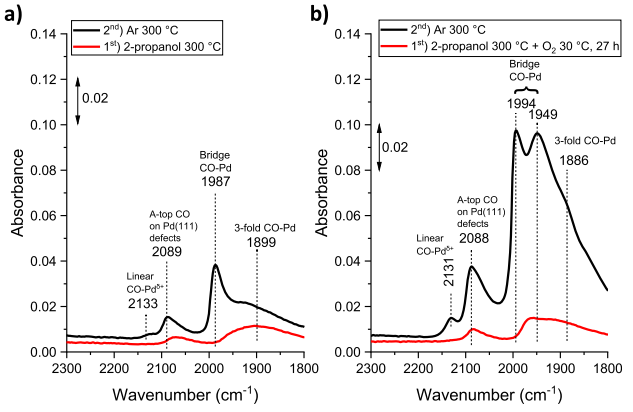

Figure 2. DRIFTS of adsorbed CO (after 10 min desorption) at 30 °C on Pd/TiO_2: (a) after treatment in 2-propanol at 300 °C (1st) and after desorption of CO at 300 °C in Ar and readsorbption (2nd); (b) after treatment in 2-propanol at 300 °C and exposure to O_2 at 30 °C for 27 h (1st) and after desorbtion of CO at 300 °C in Ar and readsorbtion (2nd). All spectra in (a) and (b) were collected for the same sample load.

to O_2 at 30 °C for 27 h was done before readsorption (Figure 2b), the amount of Pd sites exposed at the surface increased 7 times. Desorption of CO and CO_2 was monitored during exposure of the sample to O_2 at 30 °C for 27 h, and indeed, CO_x desorbs off the surface (Figure S5), which may be responsible (at least in part) for freeing Pd sites as observed in Figure 2b. CO adsorption/desorption at 30/300 °C did not affect the particle size (Figure S6), which could have affected the amount of available Pd sites.

Figure 3a shows the Pd surface sites available for CO adsorption as a function of exposure time to O_2 at 30 °C. Spectra were recorded after exposing the sample to O_2 for a certain period of time and after adsorbing/desorbing CO at 30/300 °C to remove as many carbonaceous species from the

https://dx.doi.org/10.1021/acscatal.0c05324
ACS Catal. 2021, 11, 1938−1945

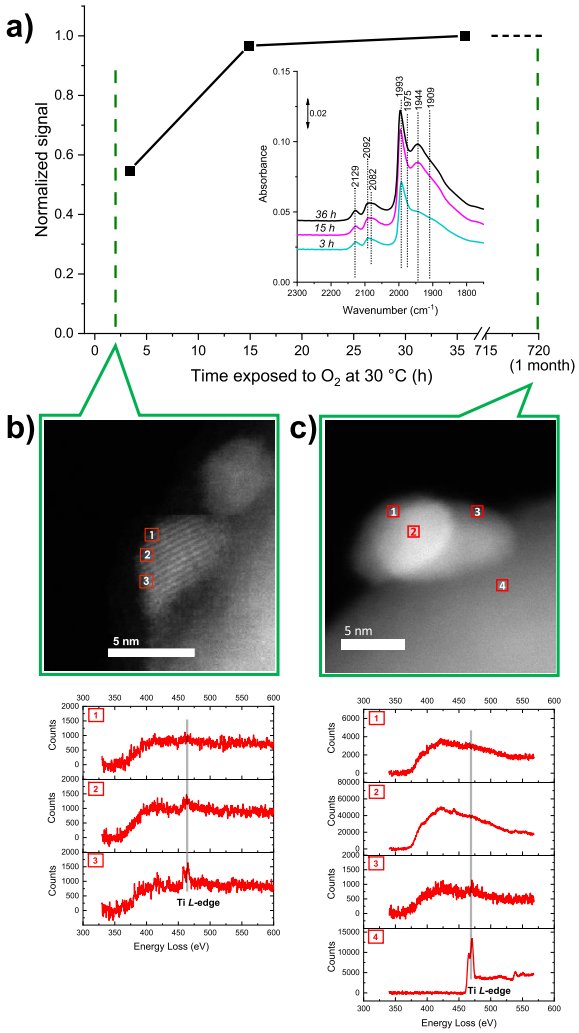

Figure 3. (a) Normalized area under IR signal from 2300 to 1800 cm^{-1} as a function of time, showing the reversibility of SMSIs upon exposure to 3% O_2/Ar at 30 °C for different periods of time on the basis of the area under the IR spectra of CO adsorption, Insert: the corresponding IR spectra of adsorbed CO at 30 °C (after 10 min desorption). CO desorbed off the sample at 300 °C in Ar before the TiO_x layer retraction was tested. (b, c) STEM images of Pd/TiO_2 treated in 2-propanol at 300 °C *ex situ* and EELS analysis (each spectrum is the sum of a 5 × 5 pixel region): (b) sample exposed to ambient air for ∼2 h between the *ex situ* treatment and an EELS analysis; (c) sample exposed to ambient air for 1 month between the *ex situ* treatment and an EELS analysis.

surface as possible. After 15 h of exposure, the overlayer covering Pd sites was almost fully retracted. Although it was shown that this overlayer is at least partially constituted by carbonaceous species, it has not been proved/disproved that a TiO_x overlayer due to SMSIs coexists.

EELS. To evaluate the existence of a TiO_x layer overcoating Pd NPs due to SMSI, we analyzed the elemental composition of the overlayer via EELS. Given the retraction of the layer overcoating Pd sites upon exposure to O_2 at room temperature, EELS was performed for 2 h (Figure 3b) and 1 month (Figure 3c) after *ex situ* 2-propanol treatment at 300 °C. For the sample analyzed 2 h after *ex situ* 2-propanol treatment, the energy loss corresponding to the Ti L-edge clearly shows that Ti is present on the Pd NPs (Figure 3b-2,3), although Ti is undetectable at the very top of the NP (Figure 3b-1), which is in agreement with a partial retraction of the TiO_x overlayer. The sample analyzed 1 month after *ex situ* 2-propanol treatment did not show Ti overcoating the Pd NPs (Figure 3c-1−3). A Ti signal was only detected on the TiO_2 support itself (Figure 3c-4). Thus, DRIFTS and EELS have shown clear evidence that Pd sites become blocked upon exposure to 2-propanol, the overlayer has the elemental composition TiO_x, and there are possibly carbonaceous species. In addition, the overlayer retracts upon exposure to air, regenerating Pd sites.

DFT Calculations. We performed DFT calculations to gain insight into whether the presence of carbon could be related to the formation of the TiO_x overlayer at such low temperature: ∼90% coverage after 2-propanol treatment at 300 °C (Figure 1) versus ∼70% coverage after H_2 treatment at 600 °C (Figure S7). To model the interface between Pd NPs covered by a reduced TiO_2 overlayer, a Ti_2O_3 monolayer was placed over the Pd surface (Figure 4). We found that carbon adsorbs the

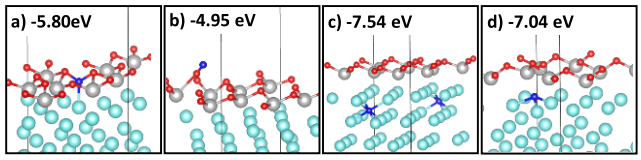

Figure 4. Adsorption energies for atomic carbon on various Ti_2O_3/Pd SMSI model systems. Color code: Pd, cyan; C, blue; O, red; Ti, gray.

strongest in the sublayers of the Pd NPs, under the Ti_2O_3 layer (Figure 4c). In other words, the SMSI structure induced by 2-propanol could be facilitated by adsorbed carbonaceous species at the interface between Pd NPs and the TiO_x overlayer. A similar adsorbate-induced SMSI has been also observed by others.[17,41]

Effect on Catalytic Performance. To gain insights into the *in situ* generation of SMSIs during catalysis, the products of 2-propanol decomposition were monitored at different reaction temperatures. Pd/TiO_2 was loaded in a plug-flow reactor, and the catalyst was pretreated *in situ* under O_2 at 295 °C for 5 h. Then, the reactor was cooled to 191 °C under an inert gas. Once the reactor temperature reached 191 °C, 2-propanol was introduced and the reaction was conducted for 9 h until a steady state was reached. Later, the reaction temperature was changed to 212, 233, and back to 212 °C. Each temperature was held for 2 h (Figure 5a). In the temperature sequence 191 °C → 212 °C → 233 °C → 212 °C (repeat), the conversion at 212 °C (repeat) drastically drops (at ∼1%), in comparison with the initial conversion (∼5%) (Figure 5b). This drop in conversion correlates with the overcoating of Pd NPs at 233 °C, which persists when the temperature is lowered to 212 °C (repeat). The different evolutions of product selectivity with time on stream for different reaction temperatures (Figure 5c) suggest that the catalyst reconstructs with changes in reaction temperature. The decay in conversion was not due to changes in particle size, as shown via TEM (Figure S8). Carbon deposits on the surface were not responsible for the decay in conversion either, as carbon deposits were nearly the same when 2-propanol interacts with the catalyst at 200 and 300 °C according to TPO experiments (Figure S9).

To shed light on the basic sites responsible for acetone production, TPD experiments with and without CO_2 adsorption at 30 °C were performed. The pretreatment at 300 °C in O_2 uncovers a minor fraction of basic sites, since

https://dx.doi.org/10.1021/acscatal.0c05324
ACS Catal. 2021, 11, 1938−1945

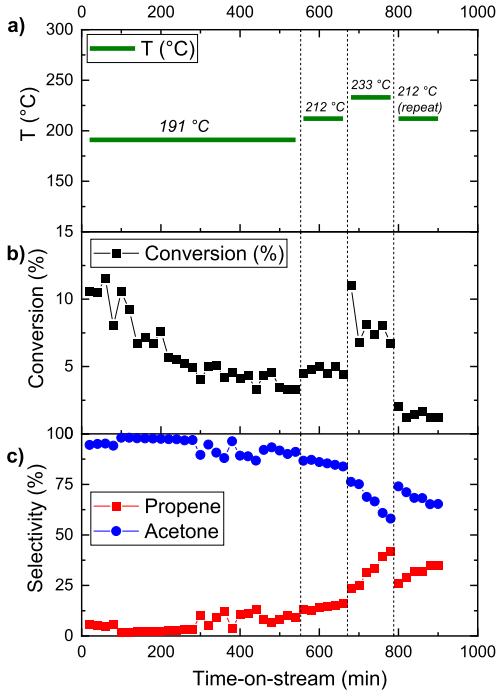

Figure 5. 2-Propanol conversion to propene and acetone over Pd/TiO_2: (a) temperature profile; (b) conversion; (c) selectivity. Reactor inlet: 0.5 μL/min 2-propanol, 50 mL/min 2% Ne/He.

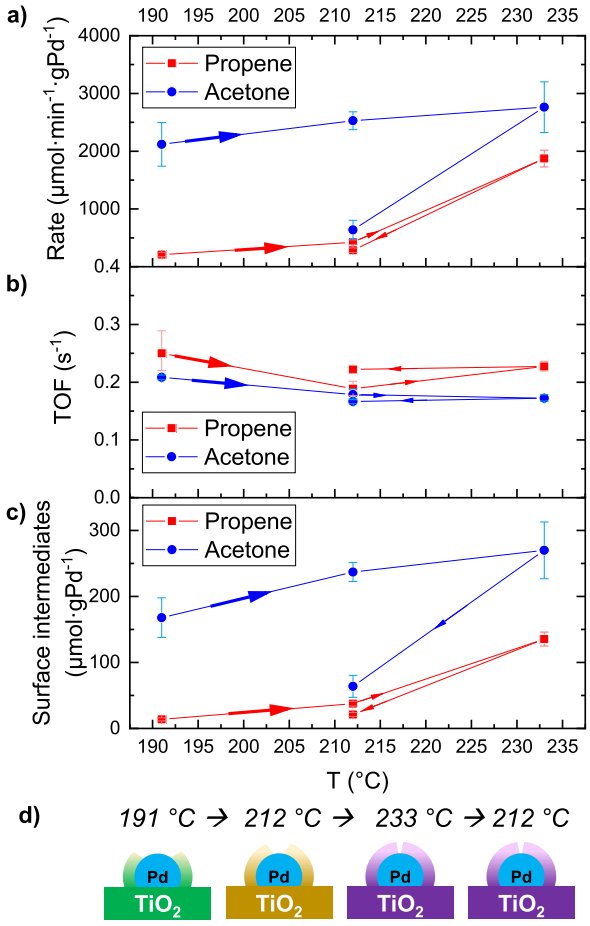

Figure 6. 2-Propanol conversion to propene and acetone over 30 mg of Pd/TiO_2: (a) steady state (or after 2 h TOS) production rates for a reactor inlet of 0.5 μL/min 2-propanol in 50 mL/min 2% Ne/He. (b) TOF measured via SSITKA; (c) surface intermediates measured via SSITKA (surface intermediates = rate (mol min^{-1} g_{Pd}^{-1})/TOF (min^{-1})); d) Sketch of SMSIs. The arrows in the lines connecting the data signal the sequence in the change of temperature: 191 °C → 212 °C → 233 °C → 212 °C.

there was not a significant number of basic sites available for CO_2 adsorption at 30 °C (Figure S10). The shape of the desorption peaks during TPD makes the quantification of the minor fraction of freed basic sites unreliable. On the other hand, TPD experiments after NH_3 adsorption at 30 °C allowed us to measure the density of acid sites. After pretreatment in O_2 at 300 °C, the Pd/TiO_2 catalyst presented 0.25 μmol of active sites per milligram of catalyst, which is 0.12 μmol/mg higher than the density of active sites on the bare TiO_2 support. Thus, the presence of Pd on the support created extra acid sites. However, after 2-propanol treatment, the surface species related to 2-propanol decomposition that remain on the surface at 300 °C (see Figure S3) possibly reduced the number of sites available to be probed with NH_3 (Figures S11 and S12). Limitations in the quantification of basic/acid sites arose from the non-*operando* nature of TPD characterization.

To provide intrinsic TOF and the density of surface intermediates leading to acetone (relatable to basic sites) and propene (related to acid sites), we performed SSITKA experiments. The gas space velocity was varied to account for product readsorption in the system (Figure S13 and Table S1).[38,39] The *in situ* generation of SMSIs affects the rates of both acetone and propene production (Figure 6a), if one compares rates when the reaction is run at 212 °C for the first time versus the second time (212 °C (repeat)). However, TOFs for acetone and propene were very similar at all temperatures studied (Figure 6b). The fact that TOFs at 212 and 212 °C (repeat) are the same, despite the conversions being significantly different, shows that differences in the rate of propene and acetone production are related to the density of active sites, *not* to the intrinsic reactivity of the sites. Figure 6c shows the density of surface intermediates (assumed to be an estimate of the surface active sites) at 212 °C, before and after an SMSI overcoating at 233 °C is formed. It is evident that the active sites for acetone production drastically decreased (from 237 to 60 μmol g_{Pd}^{-1}), suggesting that acetone is mainly produced at surface sites associated with Pd. The active sites for propene production are somewhat reduced (from 38 to 24 μmol g_{Pd}^{-1}), suggesting that interfacial Pd−Ti−O sites are the main sites for propene production. This was rationalized by considering that, when a supported metal nanoparticle is overcoated, the available Pd surface metal sites decrease more quickly in comparison to the Pd metal−support interfacial sites (Figure S14). The TiO_2 support by itself shows comparable conversion only at much higher temperature (~350 °C) (Figure S15), suggesting that only surface sites electronically or structurally affected by the presence of Pd are responsible for the turnovers reported in Figure 6.

As seen in Figure 6b, the TOFs do not have an exponential (Arrhenius-like) dependence with temperature during 2-propanol conversion over the Pd/TiO_2 catalyst. For now, we can only hypothesize that multiple active sites lead to acetone and propene production and that the *average* TOF measured via SSITKA is the result of weight averaging various types of sites, whose relative composition differs at each temperature due to *in situ* SMSIs.

https://dx.doi.org/10.1021/acscatal.0c05324
ACS Catal. 2021, 11, 1938−1945

In an additional test, we evaluated whether Pd sites become covered when the sample is exposed to 2-propanol and O_2 at 300 °C *at the same time*, since the catalytic oxidation of alcohols is a commonly studied system.[42−44] It was found that coverage of Pd sites due to *in situ* SMSIs was hindered in this case but the nature of CO adsorption on Pd sites changed significantly (Figure 7). The active sites reconstructed in the

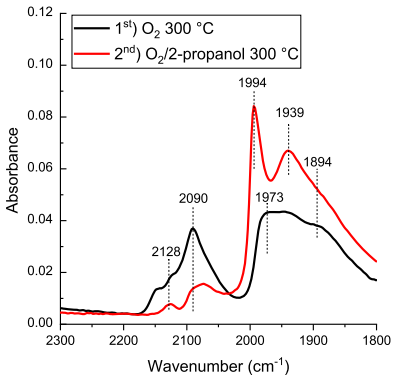

Figure 7. DRIFTS of adsorbed CO (after 10 min desorption) at 30 °C on Pd/TiO_2: (1^{st}) after treatment in O_2 at 300 °C; (2^{nd}) after treatment in an O_2/2-propanol mixture (1.8/1) at 300 °C.

presence of the alcohol in different ways depending upon the O_2 chemical potential in the reactive mixture. Further exploration on how *in situ* SMSIs change with the presence of O_2 under different conditions is of paramount importance to reveal the *operando* nature of the active sites. This endeavor lies beyond the scope of the present work.

CONCLUSIONS

The generation of SMSIs for a common catalyst, Pd/TiO_2, upon exposure to 2-propanol has been shown to occur at a temperature much lower than that in H_2 (~300 °C lower). DRIFTS of CO adsorption shows a reduction of exposed surface Pd sites by 80% when the catalyst sample is in contact with 2-propanol at 100 °C. Electron energy loss spectroscopy (EELS) shows that the support migrates over the supported NPs upon treatment in 2-propanol; however, DFT calculations suggest carbon species and reduction of the support work synergistically to induce SMSIs. Exposure of the catalyst sample to O_2 at room temperature retracted the TiO_x overlayer, reaching full retraction within ~15 h of exposure. The consequences of SMSIs on the kinetics of 2-propanol conversion reveal that apparent deactivation of the catalyst, when the reaction temperature is varied stepwise in the sequence 191 °C → 212 °C → 233 °C → 212 °C, is due to overcoating of Pd sites with a TiO_x layer. The conversion at the starting temperature of 212 °C is roughly 5 times (conversion ~5%) the conversion achieved by the sample when it is cooled back to the same reaction temperature of 212 °C (conversion ~1%). This drop in reactivity was a consequence of the expansion of the TiO_x layer covering Pd sites when the reaction temperature was 233 °C. Steady-state isotopic transient kinetic analysis (SSITKA) clearly shows that the intrinsic rate per active site does not change during this deactivation process, only the amount of active sites. The findings of this work show that, in practical applications, spikes in reactor temperature may be responsible for decreased catalytic activity due to *in situ* SMSIs formed over metal particles supported on reducible oxides.

ASSOCIATED CONTENT

Supporting Information

The Supporting Information is available free of charge at https://pubs.acs.org/doi/10.1021/acscatal.0c05324.

XRD patterns, FTIR spectroscopy, desorption plots, TEM images, particle size distribution, TPO, TPD, and SSITKA measurements, estimation of surface sites, and additional references (PDF)

AUTHOR INFORMATION

Corresponding Authors

Felipe Polo-Garzon − *Chemical Sciences Division, Oak Ridge National Laboratory, Oak Ridge, Tennessee 37831, United States;* orcid.org/0000-0002-6507-6183; Email: pologarzonf@ornl.gov

Zili Wu − *Chemical Sciences Division and Center for Nanophase Materials Sciences, Oak Ridge National Laboratory, Oak Ridge, Tennessee 37831, United States;* orcid.org/0000-0002-4468-3240; Email: wuz1@ornl.gov

Authors

Thomas F. Blum − *Center for Nanophase Materials Sciences, Oak Ridge National Laboratory, Oak Ridge, Tennessee 37831, United States*

Zhenghong Bao − *Chemical Sciences Division, Oak Ridge National Laboratory, Oak Ridge, Tennessee 37831, United States*

Kristen Wang − *Department of Chemistry, University of California, Riverside, California 92521, United States*

Victor Fung − *Center for Nanophase Materials Sciences, Oak Ridge National Laboratory, Oak Ridge, Tennessee 37831, United States;* orcid.org/0000-0002-3347-6983

Zhennan Huang − *Center for Nanophase Materials Sciences, Oak Ridge National Laboratory, Oak Ridge, Tennessee 37831, United States*

Elizabeth E. Bickel − *Department of Chemical Engineering, Tennessee Technological University, Cookeville, Tennessee 38505, United States*

De-en Jiang − *Department of Chemistry, University of California, Riverside, California 92521, United States;* orcid.org/0000-0001-5167-0731

Miaofang Chi − *Center for Nanophase Materials Sciences, Oak Ridge National Laboratory, Oak Ridge, Tennessee 37831, United States;* orcid.org/0000-0003-0764-1567

Complete contact information is available at: https://pubs.acs.org/10.1021/acscatal.0c05324

Author Contributions

All authors have given approval to the final version of the manuscript.

Notes

The authors declare no competing financial interest.

ACKNOWLEDGMENTS

This research was sponsored by the U.S. Department of Energy, Office of Science, Office of Basic Energy Sciences, Chemical Sciences, Geosciences, and Biosciences Division, Catalysis Science Program. Part of the work including IR,

kinetic measurement and electron microscopy was conducted at the Center for Nanophase Materials Sciences, which is a DOE Office of Science User Facility. This research used resources of the National Energy Research Scientific Computing Center, a DOE Office of Science User Facility. This manuscript has been authored by UT-Battelle, LLC under Contract No. DE-AC05−00OR22725 with the U.S. Department of Energy. The United States Government retains and the publisher, by accepting the article for publication, acknowledges that the United States Government retains a nonexclusive, paid-up, irrevocable, worldwide license to publish or reproduce the published form of this manuscript, or allow others to do so, for United States Government purposes. The Department of Energy will provide public access to these results of federally sponsored research in accordance with the DOE Public Access Plan (http://energy.gov/downloads/doe-public-access-plan).

REFERENCES

(1) Davis, S. E.; Ide, M. S.; Davis, R. J. Selective oxidation of alcohols and aldehydes over supported metal nanoparticles. *Green Chem.* **2013**, *15* (1), 17−45.
(2) Mattos, L. V.; Jacobs, G.; Davis, B. H.; Noronha, F. B. Production of Hydrogen from Ethanol: Review of Reaction Mechanism and Catalyst Deactivation. *Chem. Rev.* **2012**, *112* (7), 4094−4123.
(3) Albers, P.; Pietsch, J.; Parker, S. F. Poisoning and deactivation of palladium catalysts. *J. Mol. Catal. A: Chem.* **2001**, *173* (1), 275−286.
(4) Tauster, S. J.; Fung, S. C.; Garten, R. L. Strong metal-support interactions. Group 8 noble metals supported on titanium dioxide. *J. Am. Chem. Soc.* **1978**, *100* (1), 170−175.
(5) Tang, H.; Su, Y.; Zhang, B.; Lee, A. F.; Isaacs, M. A.; Wilson, K.; Li, L.; Ren, Y.; Huang, J.; Haruta, M.; Qiao, B.; Liu, X.; Jin, C.; Su, D.; Wang, J.; Zhang, T. Classical strong metal−support interactions between gold nanoparticles and titanium dioxide. *Science Advances* **2017**, *3* (10), No. e1700231.
(6) Tauster, S. J.; Fung, S. C.; Baker, R. T. K.; Horsley, J. A. Strong Interactions in Supported-Metal Catalysts. *Science* **1981**, *211* (4487), 1121−1125.
(7) Zhang, S.; Plessow, P. N.; Willis, J. J.; Dai, S.; Xu, M.; Graham, G. W.; Cargnello, M.; Abild-Pedersen, F.; Pan, X. Dynamical Observation and Detailed Description of Catalysts under Strong Metal−Support Interaction. *Nano Lett.* **2016**, *16* (7), 4528−4534.
(8) van Deelen, T. W.; Hernández Mejía, C.; de Jong, K. P. Control of metal-support interactions in heterogeneous catalysts to enhance activity and selectivity. *Nature Catalysis* **2019**, *2* (11), 955−970.
(9) Beck, A.; Huang, X.; Artiglia, L.; Zabilskiy, M.; Wang, X.; Rzepka, P.; Palagin, D.; Willinger, M.-G.; van Bokhoven, J. A. The dynamics of overlayer formation on catalyst nanoparticles and strong metal-support interaction. *Nat. Commun.* **2020**, *11* (1), 3220.
(10) Wu, Z.; Li, Y.; Huang, W. Size-Dependent Pt-TiO2 Strong Metal−Support Interaction. *J. Phys. Chem. Lett.* **2020**, *11* (12), 4603−4607.
(11) Han, B.; Guo, Y.; Huang, Y.; Xi, W.; Xu, J.; Luo, J.; Qi, H.; Ren, Y.; Liu, X.; Qiao, B.; Zhang, T. Strong Metal−Support Interactions between Pt Single Atoms and TiO2. *Angew. Chem., Int. Ed.* **2020**, *59* (29), 11824−11829.
(12) Du, X.; Huang, Y.; Pan, X.; Han, B.; Su, Y.; Jiang, Q.; Li, M.; Tang, H.; Li, G.; Qiao, B. Size-dependent strong metal-support interaction in TiO2 supported Au nanocatalysts. *Nat. Commun.* **2020**, *11* (1), 5811.
(13) Tang, H.; Su, Y.; Guo, Y.; Zhang, L.; Li, T.; Zang, K.; Liu, F.; Li, L.; Luo, J.; Qiao, B.; Wang, J. Oxidative strong metal−support interactions (OMSI) of supported platinum-group metal catalysts. *Chemical Science* **2018**, *9* (32), 6679−6684.
(14) Zhang, J.; Wang, H.; Wang, L.; Ali, S.; Wang, C.; Wang, L.; Meng, X.; Li, B.; Su, D. S.; Xiao, F.-S. Wet-Chemistry Strong Metal−Support Interactions in Titania-Supported Au Catalysts. *J. Am. Chem. Soc.* **2019**, *141* (7), 2975−2983.
(15) Campbell, C. T. Electronic perturbations. *Nat. Chem.* **2012**, *4*, 597.
(16) Cargnello, M.; Jaén, J. J. D.; Garrido, J. C. H.; Bakhmutsky, K.; Montini, T.; Gámez, J. J. C.; Gorte, R. J.; Fornasiero, P. Exceptional Activity for Methane Combustion over Modular Pd@CeO_2 Subunits on Functionalized Al_2O_3. *Science* **2012**, *337* (6095), 713.
(17) Matsubu, J. C.; Zhang, S.; DeRita, L.; Marinkovic, N. S.; Chen, J. G.; Graham, G. W.; Pan, X.; Christopher, P. Adsorbate-mediated strong metal−support interactions in oxide-supported Rh catalysts. *Nat. Chem.* **2017**, *9*, 120.
(18) Ro, I.; Resasco, J.; Christopher, P. Approaches for Understanding and Controlling Interfacial Effects in Oxide-Supported Metal Catalysts. *ACS Catal.* **2018**, *8* (8), 7368−7387.
(19) Zhang, Y.; Yang, X.; Yang, X.; Duan, H.; Qi, H.; Su, Y.; Liang, B.; Tao, H.; Liu, B.; Chen, D.; Su, X.; Huang, Y.; Zhang, T. Tuning reactivity of Fischer−Tropsch synthesis by regulating TiOx overlayer over Ru/TiO2 nanocatalysts. *Nat. Commun.* **2020**, *11* (1), 3185.
(20) Matsubu, J. C.; Zhang, S.; DeRita, L.; Marinkovic, N. S.; Chen, J. G.; Graham, G. W.; Pan, X.; Christopher, P. Adsorbate-mediated strong metal−support interactions in oxide-supported Rh catalysts. *Nat. Chem.* **2017**, *9* (2), 120−127.
(21) Polo-Garzon, F.; Blum, T. F.; Fung, V.; Bao, Z.; Chen, H.; Huang, Z.; Mahurin, S. M.; Dai, S.; Chi, M.; Wu, Z. Alcohol-Induced Low-Temperature Blockage of Supported-Metal Catalysts for Enhanced Catalysis. *ACS Catal.* **2020**, *10*, 8515−8523.
(22) Zhang, J.; Wang, B.; Nikolla, E.; Medlin, J. W. Directing Reaction Pathways through Controlled Reactant Binding at Pd−TiO2 Interfaces. *Angew. Chem., Int. Ed.* **2017**, *56* (23), 6594−6598.
(23) Sun, J.; Han, Y.; Fu, H.; Qu, X.; Xu, Z.; Zheng, S. Au@Pd/TiO2 with atomically dispersed Pd as highly active catalyst for solvent-free aerobic oxidation of benzyl alcohol. *Chem. Eng. J.* **2017**, *313*, 1−9.
(24) Wrasman, C. J.; Boubnov, A.; Riscoe, A. R.; Hoffman, A. S.; Bare, S. R.; Cargnello, M. Synthesis of Colloidal Pd/Au Dilute Alloy Nanocrystals and Their Potential for Selective Catalytic Oxidations. *J. Am. Chem. Soc.* **2018**, *140* (40), 12930−12939.
(25) Bhogeswararao, S.; Srinivas, D. Catalytic conversion of furfural to industrial chemicals over supported Pt and Pd catalysts. *J. Catal.* **2015**, *327*, 65−77.
(26) Pei, G. X.; Liu, X. Y.; Wang, A.; Lee, A. F.; Isaacs, M. A.; Li, L.; Pan, X.; Yang, X.; Wang, X.; Tai, Z.; Wilson, K.; Zhang, T. Ag Alloyed Pd Single-Atom Catalysts for Efficient Selective Hydrogenation of Acetylene to Ethylene in Excess Ethylene. *ACS Catal.* **2015**, *5* (6), 3717−3725.
(27) Biffis, A.; Centomo, P.; Del Zotto, A.; Zecca, M. Pd Metal Catalysts for Cross-Couplings and Related Reactions in the 21st Century: A Critical Review. *Chem. Rev.* **2018**, *118* (4), 2249−2295.
(28) Wang, J.; Chen, H.; Hu, Z.; Yao, M.; Li, Y. A Review on the Pd-Based Three-Way Catalyst. *Catal. Rev.: Sci. Eng.* **2015**, *57* (1), 79−144.
(29) Mimura, N.; Hiyoshi, N.; Daté, M.; Fujitani, T.; Dumeignil, F. Microscope Analysis of Au−Pd/TiO2 Glycerol Oxidation Catalysts Prepared by Deposition−Precipitation Method. *Catal. Lett.* **2014**, *144* (12), 2167−2175.
(30) Ward, T.; Delannoy, L.; Hahn, R.; Kendell, S.; Pursell, C. J.; Louis, C.; Chandler, B. D. Effects of Pd on Catalysis by Au: CO Adsorption, CO Oxidation, and Cyclohexene Hydrogenation by Supported Au and Pd−Au Catalysts. *ACS Catal.* **2013**, *3* (11), 2644−2653.
(31) Lopez-Sanchez, J. A.; Dimitratos, N.; Glanville, N.; Kesavan, L.; Hammond, C.; Edwards, J. K.; Carley, A. F.; Kiely, C. J.; Hutchings, G. J. Reactivity studies of Au−Pd supported nanoparticles for catalytic applications. *Appl. Catal., A* **2011**, *391* (1), 400−406.
(32) Kresse, G.; Furthmüller, J. Efficiency of ab-initio total energy calculations for metals and semiconductors using a plane-wave basis set. *Comput. Mater. Sci.* **1996**, *6* (1), 15−50.

https://dx.doi.org/10.1021/acscatal.0c05324
ACS Catal. 2021, 11, 1938−1945

(33) Kresse, G.; Furthmuller, J. Efficient iterative schemes for ab initio total-energy calculations using a plane-wave basis set. *Phys. Rev. B: Condens. Matter Mater. Phys.* **1996**, *54* (16), 11169−11186.
(34) Perdew, J. P.; Burke, K.; Ernzerhof, M. Generalized Gradient Approximation Made Simple. *Phys. Rev. Lett.* **1996**, *77* (18), 3865−3868.
(35) Kresse, G.; Joubert, D. From ultrasoft pseudopotentials to the projector augmented-wave method. *Phys. Rev. B: Condens. Matter Mater. Phys.* **1999**, *59* (3), 1758−1775.
(36) Blochl, P. E. PROJECTOR AUGMENTED-WAVE METHOD. *Phys. Rev. B: Condens. Matter Mater. Phys.* **1994**, *50* (24), 17953−17979.
(37) Bao, Z.; Fung, V.; Polo-Garzon, F.; Hood, Z. D.; Cao, S.; Chi, M.; Bai, L.; Jiang, D.-e.; Wu, Z. The interplay between surface facet and reconstruction on isopropanol conversion over SrTiO3 nanocrystals. *J. Catal.* **2020**, *384*, 49−60.
(38) Ledesma, C.; Yang, J.; Chen, D.; Holmen, A. Recent Approaches in Mechanistic and Kinetic Studies of Catalytic Reactions Using SSITKA Technique. *ACS Catal.* **2014**, *4* (12), 4527−4547.
(39) Shannon, S. L.; Goodwin, J. G. Characterization of Catalytic Surfaces by Isotopic-Transient Kinetics during Steady-State Reaction. *Chem. Rev.* **1995**, *95* (3), 677−695.
(40) Wang, X.; Wu, G.; Guan, N.; Li, L. Supported Pd catalysts for solvent-free benzyl alcohol selective oxidation: Effects of calcination pretreatments and reconstruction of Pd sites. *Appl. Catal., B* **2012**, *115*−*116*, 7−15.
(41) Liu, S.; Xu, W.; Niu, Y.; Zhang, B.; Zheng, L.; Liu, W.; Li, L.; Wang, J. Ultrastable Au nanoparticles on titania through an encapsulation strategy under oxidative atmosphere. *Nat. Commun.* **2019**, *10* (1), 5790.
(42) Mallat, T.; Baiker, A. Oxidation of Alcohols with Molecular Oxygen on Solid Catalysts. *Chem. Rev.* **2004**, *104* (6), 3037−3058.
(43) Parmeggiani, C.; Matassini, C.; Cardona, F. A step forward towards sustainable aerobic alcohol oxidation: new and revised catalysts based on transition metals on solid supports. *Green Chem.* **2017**, *19* (9), 2030−2050.
(44) Ali, M. E.; Rahman, M. M.; Sarkar, S. M.; Hamid, S. B. A. Heterogeneous metal catalysts for oxidation reactions. *J. Nanomater.* **2014**, *2014*, 192038.

https://dx.doi.org/10.1021/acscatal.0c05324
ACS Catal. 2021, 11, 1938−1945